Cureus
Part of SPRINGER NATURE

Open Access Original Article

Mechanical Effects of a Design Opening in a Three-Dimensional-Printed Mallet Finger Orthosis: A Finite-Element Study

Review began 09/28/2026
Review ended 10/28/2026
Published 11/11/2026

© **Copyright** 2026
Sedigh et al. This is an open access article distributed under the terms of the Creative Commons Attribution License CC-BY 4.0., which permits unrestricted use, distribution, and reproduction in any medium, provided the original author and source are credited.

DOI: 10.7759/cureus.119498

Ashkan Sedigh [1], Kirk Beredjiklian [2], Nathan Pentecost [2], Ainsley Arquitola [2], Pranavi Jonnalagadda [2], Praneel Chundru [3], Michael Rivlin [3], Pedro Beredjiklian [3]

1. Department of Mechanical Engineering, Villanova University, Villanova, USA 2. Department of Orthopedics, Dimension Ortho, Philadelphia, USA 3. Department of Hand Surgery, Rothman Orthopedic Institute, Philadelphia, USA

Corresponding author: Pedro Beredjiklian, pedro.beredjiklian@rothmanortho.com

Abstract

Background: Mallet finger is commonly managed by immobilizing the distal interphalangeal (DIP) joint in extension. Three-dimensional (3D) printing enables customized orthoses, but geometric features introduced for access, ventilation, or comfort may alter device mechanics. This study used finite-element (FE) analysis to quantify the mechanical effect of a longitudinal vent in a 3D-printed mallet finger orthosis.

Methods: Two orthosis geometries, one with a 26.2 mm × 7.6 mm longitudinal vent and one without the vent, were evaluated under axial compression and anatomical DIP loading. Peak effective stress was compared under axial compression, while maximum principal stress (MPS) and lateral displacement were evaluated under DIP loading. Mesh sensitivity was assessed using MPS sampled at a consistent DIP joint location across progressively refined meshes.

Results: Under axial compression, peak effective stress decreased from 4.409 MPa in the orthosis with the vent to 3.409 MPa in the orthosis without the vent, representing a 22.7% reduction. Under anatomical DIP loading, MPS decreased from 0.2554 to 0.1331 MPa, representing a 47.9% reduction, while the maximum displayed lateral displacement decreased from 1.957×10^{-3} to 6.518×10^{-4} mm, representing a 66.7% reduction.

Conclusion: Under the evaluated conditions, the longitudinal vent increased stress concentration and deformation in the 3D-printed mallet splint. However, the stresses remained well below the measured material strength. Vent design should balance structural performance with the clinical benefits of ventilation. Future clinical studies are needed before further design recommendations can be made.

Categories: Trauma, Physical Medicine & Rehabilitation, Orthopedics
Keywords: 3d printing, additive manufacturing, dip joint, finite-element analysis, mallet finger, orthosis, splint, stress concentration

Introduction

Mallet finger results from disruption of the terminal extensor mechanism at the distal phalanx and results in an inability to actively extend the distal interphalangeal (DIP) joint. There is no defined, universally accepted treatment for mallet finger, though a general consensus agrees on orthotic treatment [1-3]. Nonoperative immobilization remains a primary treatment approach for most acute mallet injuries, with continuous splinting of the DIP joint in extension as an effective treatment strategy [2,4].

Although many splint configurations are used clinically, orthosis fit, comfort, skin tolerance, and adherence to the prescribed remain important considerations. A systematic review reported that custom-made finger orthoses may reduce skin complications compared with prefabricated devices while producing similar clinical outcomes [5,6]. More recent work has explored three-dimensional (3D)-printed mallet finger orthoses as a means of producing personalized devices with reproducible geometry, low material use, and rapid fabrication [7]. A national survey found that many healthcare professionals have not been fully aware of the benefits of 3D printing, although, despite their limited knowledge, they developed a positive attitude toward future implementation [1].

Previous work on 3D printing for mallet finger has included testing in patient care [8]. Other investigators have developed patient-specific 3D-printed orthoses as alternatives to conventional prefabricated Stack and aluminum-foam (Zimmer, Zimmer Biomet Holdings, Inc., Warsaw, IN) splints, which may be limited by standardized sizing, fit, comfort, and skin-related complications [7-9]. Hou et al. tested their splint on qualitative factors such as comfort, skin maceration, and splint fit, along with quantitative factors like angle of finger extension. The most common difficulties with the splint were hand hygiene and activities, such as gripping objects. While attention has been directed toward customization and adjustability of the orthoses,

lower priority was placed on geometric modifications, such as vents, that influence the structural behavior of the orthoses [10].

3D printing also creates the opportunity to incorporate vents, cutouts, or topology-optimized regions intended to improve access, ventilation, weight, or comfort. However, material removal changes the structural load path and may create local stress concentrations. Previous engineering work on patient-specific 3D-printed mallet splints demonstrated that finite-element (FE) analysis can be used to quantify orthosis stress and deflection and to guide geometry optimization [7,9]. A recent review concluded that evidence on 3D-printed mallet orthoses remains limited and heterogeneous, with a need for stronger mechanical and clinical evaluation [1,11].

Additionally, 3D printing offers several advantages for orthopedic immobilization, including patient-specific customization, rapid digital fabrication, improved ventilation and washability, and the ability to modify device geometry based on anatomical and mechanical requirements. Previous studies demonstrated that 3D-printed polymers can provide mechanical properties suitable for orthoses while enabling customized and remotely fabricated splints that may reduce the need for conventional in-person casting and fitting workflows [12-14]. Previously published work by our group has shown that 3D-printed upper extremity casts can provide clinically appropriate immobilization and wear comfort compared with conventional alternatives, while prior clinical and mechanical studies have demonstrated the feasibility of 3D printing for customized orthoses, including improved comfort and comparable mechanical properties [13,15,16]. Collectively, these studies support the use of 3D printing as a platform for developing lightweight, reproducible, and anatomically customized orthoses while also enabling systematic modification of features such as vents, thickness variation, and structural geometry to improve device performance. However, 3D-printed orthoses also have limitations, including cost, the need for specialized equipment and expertise, fabrication time compared with conventional splints, and limited clinical evidence comparing outcomes [1].

The purpose of the present study was to determine how a vent affects stress and displacement in a 3D-printed mallet finger orthosis. We hypothesized that a vent would increase local stress concentration and deformation compared with the no-vent design.

Materials And Methods

Orthosis geometries

Two mallet finger orthosis geometries were evaluated: (1) a baseline device without a vent and (2) an otherwise comparable device containing a vent measuring 26.2 mm in length and 7.6 mm in width (see the Appendix). The remaining overall geometry was maintained for the comparison. A 26.2 mm × 7.6 mm longitudinal vent was included as a design feature potentially relevant to access and ventilation. These dimensions were specific to the investigated geometry and were not mechanically optimized. The two models were imported as surface geometry and prepared for FE meshing and 3D printing (Figure *1*). The longitudinal vent had rounded edges. The orthosis edges were smoothed using a 0.25 mm fillet radius to reduce sharp geometric transitions and improve mesh quality. The vent was located on the volar surface and extended from 13.1 mm above the middle phalanx to 13.1 mm below relative to the DIP joint. The orthosis had a nominal wall thickness of 1.5 mm, which was maintained consistently between the vented and unvented configurations.

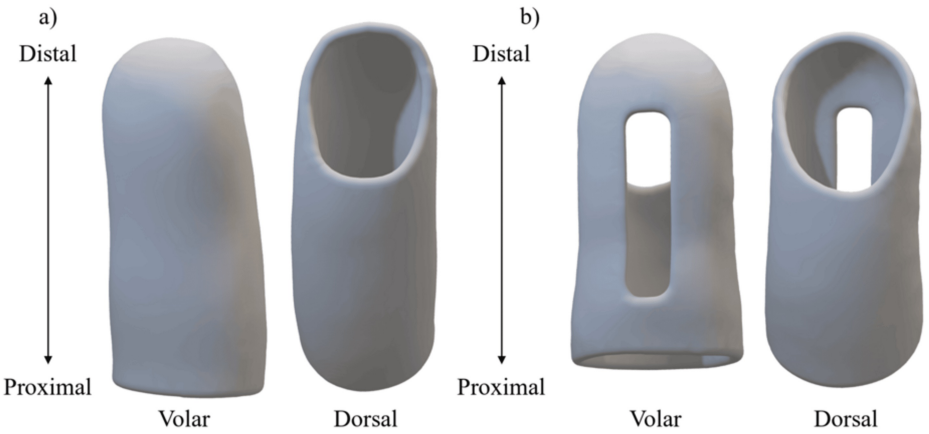


FIGURE 1: Mallet finger orthosis geometries used in the finite-element analysis. (a) Orthosis without the longitudinal vent. (b) Orthosis with the longitudinal vent. Proximal/distal and dorsal/volar orientation labels are provided to clarify the anatomical orientation of the orthoses, with the vent located on the volar side

Flexural material characterization

Flexural properties of the printed materials were characterized using three-point bending in accordance with ASTM D790-25, Procedure A. A support span-to-thickness ratio of 16:1 was used. The support span was 1.97 in. (50.0 mm), and the crosshead rate was 0.053 in./minute (1.35 mm/minute).

Before testing, specimens were conditioned for at least 40 hours at 23°C ± 2°C and 50% ± 10% relative humidity in accordance with ASTM D618-21. Mechanical testing was performed at an ambient temperature of 24.0°C and 56.0% relative humidity. Flexural strength and flexural modulus were calculated from the three-point bending tests according to ASTM D790-25.

Material model and manufacturing information

The proprietary nanocopper orthosis material was modeled as a homogeneous elastic material. The orthoses were manufactured using a commercially available polylactic acid (PLA)-based filament containing nano-copper additives, supplied by Copper3D (Santiago, Chile). The composition and antimicrobial characteristics of Copper3D's PLA-based nano-copper materials have been previously investigated [17]. The material was modeled as homogeneous and linearly elastic, with an experimentally determined mean flexural modulus of 2.03 ± 0.03 GPa from ASTM D790-25 three-point bending tests. The orthoses were fabricated using fused deposition modeling (FDM) technology with a Delta-configuration 3D printer and PLA-based nanocopper filament supplied by Copper3D. A layer height of 0.2 mm and a nozzle diameter of 4 mm were used. The orthoses were printed without internal infill (0%), with structural integrity provided by the continuous printed walls.

A Poisson’s ratio of 0.36 was assigned. The available three-specimen flexural test set yielded a mean flexural modulus of 295 ± 3.82 ksi (2.03 ± 0.03 GPa). A Poisson's ratio of 0.36 was adopted from previously published FE studies of 3D-printed PLA [18]. This value was assumed based on the PLA base polymer and was not independently measured for the nano-copper-containing filament. The flexural test specimens were fabricated using the same FDM printing parameters and build orientation as the orthoses to ensure consistent manufacturing conditions.

FE model

FE simulations were performed using FEBioStudio (version 3.2.0; FEBio Software Suite, Salt Lake City, UT) [19]. The orthosis was discretized using 10-node quadratic tetrahedral solid elements, along with approximately three to four elements through the 1.5 mm wall thickness to resolve stress gradients, particularly near the DIP loading region and vent margins.

Two loading conditions were evaluated: axial compression and anatomical DIP loading. The axial compression condition was designed to simulate mechanical compression testing using a universal testing machine. A uniformly distributed pressure of 0.146 MPa, calculated by dividing the applied compressive force by the loaded surface area, was applied to the tip of the orthosis along its longitudinal axis, while the opposing end was fully constrained in three directions (Figure *2a*). The second represented an anatomical

loading condition associated with DIP extension. Identical loading and boundary conditions were applied to both orthosis geometries within each load case so that differences could be attributed to device geometry. For the axial compression loading condition, a compressive load of 2N was distributed over the terminal surface of the orthosis along its longitudinal axis [20], while the distal end was constrained [7]. Figure 2 summarizes the boundary conditions used for axial compression and anatomical DIP loading.

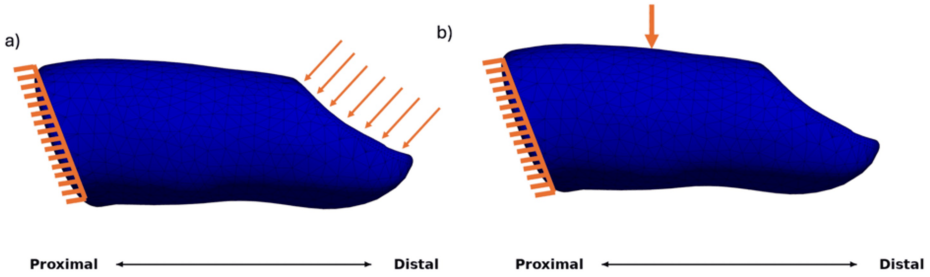


FIGURE 2: Finite-element boundary conditions for (a) axial compression and (b) anatomical DIP loading. Identical loading and boundary conditions were applied to the two orthosis geometries within each loading case. Proximal/distal and dorsal/volar orientation labels are included to clarify the anatomical orientation and boundary conditions

DIP: distal interphalangeal

Mesh sensitivity analysis

A mesh sensitivity analysis was performed using the vented orthosis under the same DIP loading condition. Three progressively refined meshes were evaluated: the current study mesh (20,891 elements; 6,680 nodes), a higher density mesh (167,128 elements; 40,295 nodes), and the highest density mesh (1,337,024 elements; 271,891 nodes). To avoid using global peak values that can be dominated by geometric discontinuities, maximum principal stress (MPS) was sampled at the same anatomically relevant location at the DIP joint for all three meshes.

Outcome measures and comparison

For axial compression, the primary FE outcome was peak effective stress within the orthosis. For anatomical DIP loading, MPS and lateral displacement were evaluated. Lateral displacement was reported to capture out-of-plane deformation introduced by the asymmetric vent. For each loading condition, the percentage reduction associated with removing the vent was calculated as follows:

$$\text{Reduction (\%)} = \left[\frac{\sigma_{\text{vent}} - \sigma_{\text{no-vent}}}{\sigma_{\text{vent}}}\right] \times 100$$

Stress contour maps were compared qualitatively to identify regions of stress concentration. Under DIP loading, the maximum displayed lateral displacement was also recorded from the FE results. Contact pressure was not calculated because the present device-level model did not include an anatomically accurate finger-orthosis contact representation.

Results

Flexural material characterization

For the three-specimen test set provided for material characterization, all specimens had a reported cross-sectional area of 0.058 in^2. Maximum load ranged from 14.4 to 18.4 lbf, with a mean of 16.0 ± 2.11 lbf (71.2 ± 9.4 N). Flexural strength ranged from 5,870 to 7,500 psi, with a mean of 6,520 ± 868 psi (45.0 ± 6.0 MPa). Flexural modulus ranged from 291 to 298 ksi, with a mean of 295 ± 3.82 ksi (2.03 ± 0.03 GPa). Individual specimen results are summarized in Table 1.

Specimen	Area (mm²)	Flexural strength (MPa)	Flexural modulus (GPa)
A	37.42	40.47	2.048
B	37.42	42.68	2.006
C	37.42	51.71	2.055
Mean	37.42	44.95	2.034
Standard deviation	0.00	5.98	0.026

TABLE 1: Flexural properties obtained from three-point bending according to ASTM D790-25, procedure A

Mesh sensitivity

DIP-joint MPS increased from 0.131 to 0.172 to 0.183 MPa as the mesh increased from 20,891 to 167,128 to 1,337,024 elements. Although the raw change between the two finest meshes remained 6.4%, the element-count-normalized sensitivity decreased to 0.91% per 100% increase in element count, compared with 4.47% during the preceding refinement. The raw change in MPS between the current study and higher density meshes was 6.4% and between the higher and highest density meshes was 4.4%. The marked reduction in both raw and normalized sensitivity indicates that the DIP-joint stress response was approaching mesh stability at the highest density.

Device comparison under the first loading condition

Under axial compression, the vented orthosis reached a peak effective stress of 4.409 MPa, whereas the unvented orthosis reached 3.409 MPa. Removing the vent therefore reduced peak effective stress by 1.000 MPa, corresponding to a 22.7% reduction relative to the vented configuration.

The effective-stress contours demonstrated elevated local stress adjacent to the opening in the vented design. In the unvented configuration, stress was distributed across a continuous wall without the same local geometric discontinuity. Under axial compression, the maximum effective stress occurred at the constrained proximal rim in the unvented orthosis (3.409 MPa), whereas the vented orthosis exhibited a higher peak stress (4.409 MPa) around the vent margins (Figure *3*).

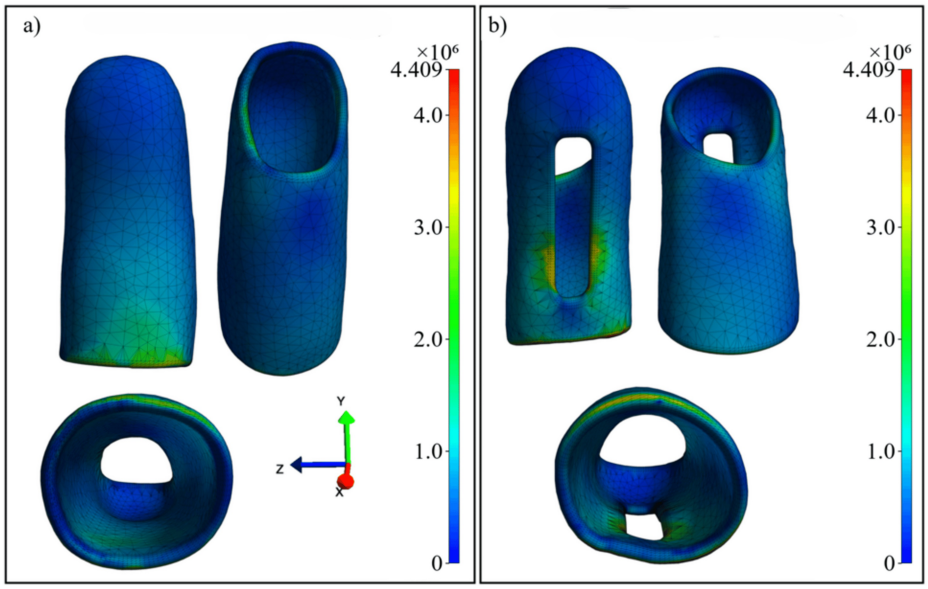


FIGURE 3: Effective-stress contours under axial compression for (a) the orthosis without the vent and (b) the orthosis with the vent. The displayed peak effective stresses were 3.409 and 4.409 MPa, respectively

Anatomical DIP loading

The difference between designs was larger under anatomical DIP loading. MPS was 0.2554 MPa for the orthosis with the vent and 0.1331 MPa for the orthosis without the vent. This represents an absolute reduction of 0.1223 MPa and a relative reduction of 47.9%. The maximum displayed lateral displacement decreased from 1.957×10^{-3} mm in the vented design to 6.518×10^{-4} mm in the unvented design, corresponding to a 66.7% reduction.

Under anatomical DIP loading, the peak MPS occurred in the DIP-joint region for both configurations. The vented orthosis exhibited a higher peak MPS of 0.2554 MPa compared with 0.1331 MPa in the unvented orthosis, indicating that the longitudinal vent altered the local load distribution and increased stress concentration near the DIP joint. The vented model exhibited higher MPS and greater lateral displacement under the same DIP loading condition. Figures *4*, *5* show the maximum principal stress and lateral-displacement distributions for the two configurations, respectively.

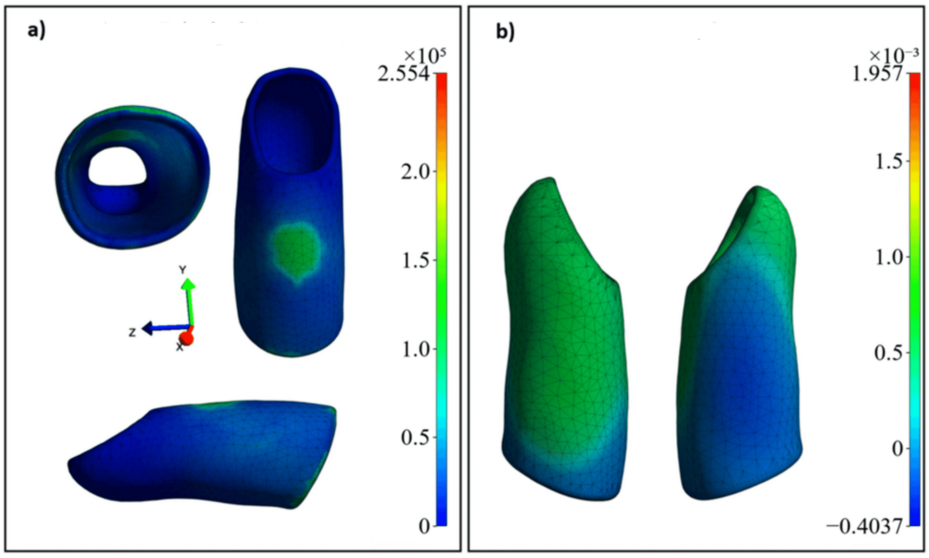


FIGURE 4: Finite element stress and displacement distributions in the unvented mallet finger orthosis under anatomical DIP joint loading. (a) Maximum principal stress (Pa), shown in multiple views. (b) Signed lateral displacement (mm), shown from two lateral perspectives

DIP: distal interphalangeal

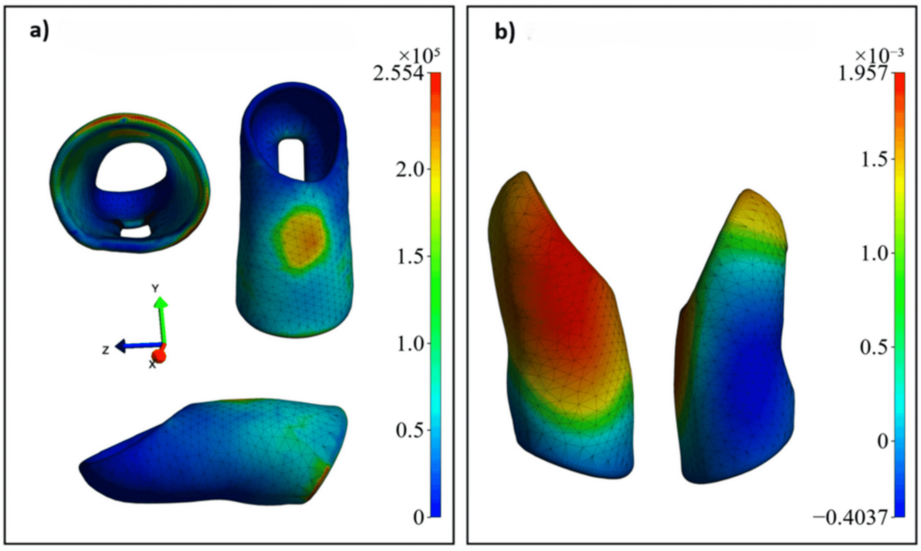


FIGURE 5: Finite element stress and displacement distributions in the vented mallet finger orthosis under anatomical DIP joint loading. (a) Maximum principal stress (Pa), shown in multiple views. (b) Signed lateral displacement (mm), shown from two lateral perspectives

DIP: distal interphalangeal

Comparison across loading conditions

Both loading conditions produced the same directional result: removing the vent reduced the principal mechanical response of the orthosis. Under axial compression, peak effective stress decreased by 22.7%. Under anatomical DIP loading, MPS decreased by 47.9%, and the maximum displayed lateral displacement decreased by 66.7%. These consistent directional differences support the interpretation that the vent is a meaningful geometric contributor to local stress concentration and device deformation rather than an isolated numerical effect (Table *2*). Relative to the measured flexural strength of 45.0 MPa, safety factors under axial compression were 10.2 for the vented design and 13.2 for the unvented design, and under DIP loading were 176 and 338, respectively.

Loading condition/outcome	Vented	Unvented	Absolute reduction	Relative reduction (%)	No-vent/vent ratio
Axial compression, peak effective stress (MPa)	4.409	3.409	1.000 MPa	22.7	0.773
Anatomical DIP loading, MPS (MPa)	0.2554	0.1331	0.1223 MPa	47.9	0.521
Anatomical DIP loading, max. lateral displacement (mm)	1.957×10^{-3}	6.518×10^{-4}	1.305×10^{-3} mm	66.7	0.333

TABLE 2: Comparison of finite-element outcomes between orthosis designs

MPS: maximum principal stress; DIP: distal interphalangeal

Discussion

The principal finding of this study is that the longitudinal vent substantially altered the mechanical response of the mallet finger orthosis. Under axial compression, the unvented configuration reduced peak effective stress by 22.7%. Under anatomical DIP loading, removal of the vent reduced MPS by 47.9% and the maximum displayed lateral displacement by 66.7%. The consistency of these findings across different loading conditions and outcome measures indicates that even a localized geometric feature can meaningfully change the stress distribution and deformation of a thin-walled finger orthosis.

Experimental flexural characterization provides a material-property basis for the computational model. The

available three-specimen test set produced a mean flexural modulus of 2.03 GPa with low between-specimen variability (standard deviation = 0.03 GPa). This reduces reliance on nominal manufacturer values.

The mesh-sensitivity analysis supports the stability of the anatomically relevant DIP-joint stress trend with progressive refinement. DIP-joint MPS increased from 0.131 to 0.172 to 0.183 MPa as the mesh increased from 20,891 to 167,128 to 1,337,024 elements. Although the raw change between the two finest meshes remained 6.4%, the element-count-normalized sensitivity decreased to 0.91% per 100% increase in element count, compared with 4.47% during the preceding refinement. This diminishing sensitivity suggests that the local DIP-joint response was approaching mesh stability while avoiding reliance on global peaks near geometric discontinuities. Mechanically, the observed design effect is consistent with classical stress-concentration behavior: a vent interrupts the continuous load path and creates edges at which stress can localize. Under DIP loading, the vent reduces the available cross-sectional area and redirects load around its perimeter, whereas removing the vent restores a more continuous structural path and reduces both stress and deformation.

The present findings should be considered in the context of previous 3D-printed mallet orthosis research. A prior study used FE analysis and topology optimization to study patient-specific mallet splints and showed that material distribution directly affects stress and deflection [7]. Their work illustrates that material removal can be beneficial when it is distributed through a controlled optimization strategy. In contrast, the present results suggest that a discrete vent placed in a mechanically active region can act as a local stress concentrator. Therefore, the mechanical effect of material removal depends not only on the amount of material removed but also on the location, shape, and load path surrounding the feature.

From a design perspective, the results do not imply that vents should be eliminated. Vents may provide clinical benefits such as access, ventilation, weight reduction, cleaning, or patient comfort. Previous work on customized mallet orthoses has emphasized comfort, individualized fit, and skin tolerance as important advantages of custom devices. The design decision is therefore a tradeoff between structural performance and user-related benefits. The present FE analysis provides a quantitative basis for that tradeoff by identifying the mechanical penalty associated with the current vent geometry. Rather than eliminating ventilation, future designs may optimize vent location and geometry or reinforce regions of high stress.

The vent may also carry clinical risks not captured by this analysis. The finger pulp is highly compliant, and post-traumatic swelling is common, so a sizeable opening in a rigid shell may allow soft tissue to bulge into the vent, while its margins may concentrate pressure on the skin over several weeks of continuous wear. Although two volunteers wore the orthoses for a preliminary assessment of fit and comfort, no formal skin-response evaluation was performed, and the model did not include soft tissues or finger-orthosis contact. Multiple smaller perforations may provide ventilation with a lower risk of soft-tissue herniation and should be evaluated in future work.

The study also highlights an important distinction between device stress and finger contact pressure. The FE outputs evaluated here were effective stress within the orthosis under axial compression and MPS and displacement under anatomical DIP loading. Lower device stress or displacement does not, by itself, demonstrate lower pressure on the skin or distal phalanx. Direct assessment of contact pressure would require an anatomically representative finger model, appropriate soft-tissue material properties, and explicit contact interactions between the finger and orthosis.

The present study has several limitations. First, the analysis compared a limited number of orthosis geometries and therefore does not establish an optimal vent size or location. Second, the current model evaluates stress and displacement within the orthosis and does not directly quantify finger-orthosis contact pressure. The anatomical representation of the finger was simplified or absent in this device-level analysis; therefore, the findings primarily characterize orthosis mechanics rather than tissue-level biomechanics. In addition, the DIP load was based on extension strength, whereas loads on a mallet orthosis in clinical use may arise primarily from flexion forces, and the distal constraint differs from the three-point support used clinically. Although material properties were experimentally characterized using ASTM D790-25 three-point bending strength, the FE constitutive model remains an idealization of the printed polymer. Additionally, flexural properties were characterized from three specimens, fewer than the five specified by ASTM D790. Three-dimensional printed materials may exhibit anisotropy and may be influenced by print orientation, layer height, raster pattern, specimen thickness, and manufacturing conditions [21-23], while flexural modulus reflects the global bending response of the printed specimen and may not fully represent tensile, compressive, or direction-dependent behavior within the orthosis [24]. Finally, patient-related outcomes such as skin condition, comfort, and adherence were not assessed. Clinical studies are needed before recommending changes to ventilation design. Fatigue, cyclic loading, moisture, and temperature were also not modeled, and the model has not been experimentally validated. The future direction of this study is to include experimental mechanical validation or patient outcomes. Moreover, future studies should incorporate patient-specific anatomical models, soft-tissue mechanical properties, and explicit contact interactions to investigate tissue-level responses and potential clinical implications of vent geometry.

Conclusions

FE analysis demonstrated that a longitudinal vent increased stress concentration and deformation in a 3D-printed mallet finger orthosis under the evaluated conditions. However, stresses remained well below the measured strength of the material. These findings suggest that orthosis vent design involves a balance between structural performance and the benefits of ventilation and skin health. Rather than eliminating ventilation, future designs may benefit from optimizing vent location and geometry. Future work should include experimental validation, anatomically accurate finger-orthosis contact modeling, and clinical evaluation before conclusions are drawn regarding tissue pressure or patient outcomes.

Appendices

INTERACTIVE MODEL 1: Mallet finger orthosis model (unvented)

View Interactive Model here: https://youtu.be/nkzzy-GfW88

INTERACTIVE MODEL 2: Vented Mallet finger orthosis design

View Interactive Model here: https://youtu.be/yQdCaDi4wXc

Additional Information

Author Contributions

All authors have reviewed the final version to be published and agreed to be accountable for all aspects of the work.

Concept and design: Praneel Chundru, Ashkan Sedigh, Kirk Beredjiklian, Nathan Pentecost, Ainsley Arquitola, Pranavi Jonnalagadda, Michael Rivlin, Pedro Beredjiklian

Drafting of the manuscript: Praneel Chundru, Ashkan Sedigh, Kirk Beredjiklian, Nathan Pentecost, Ainsley Arquitola, Pranavi Jonnalagadda, Michael Rivlin, Pedro Beredjiklian

Critical review of the manuscript for important intellectual content: Praneel Chundru, Ashkan Sedigh, Kirk Beredjiklian, Nathan Pentecost, Ainsley Arquitola, Pranavi Jonnalagadda, Michael Rivlin, Pedro Beredjiklian

Acquisition, analysis, or interpretation of data: Ashkan Sedigh, Kirk Beredjiklian, Nathan Pentecost, Ainsley Arquitola, Pranavi Jonnalagadda

Supervision: Michael Rivlin, Pedro Beredjiklian

Disclosures

Human subjects: All authors have confirmed that this study did not involve human participants or tissue. **Animal subjects:** All authors have confirmed that this study did not involve animal subjects or tissue. **Conflicts of interest:** In compliance with the ICMJE uniform disclosure form, all authors declare the following: **Payment/services info:** All authors have declared that no financial support was received from any organization for the submitted work. **Financial relationships:** Pedro Beredjiklian and Michael Rivlin declare(s) employment, a patent and stock/stock options from Dimension Ortho. **Intellectual property info:** Pedro Beredjiklian and Michael Rivlin both have patents related to the company Dimension Ortho. This work may be broadly relevant. **Other relationships:** All authors have declared that there are no other relationships or activities that could appear to have influenced the submitted work.

References

1. Cronin UM, Shannon A, Ó hAodha M, Cummins NM, O'Sullivan A, O'Sullivan L: What is known from the existing literature about the treatment of mallet injury using 3D-printed splints? A scoping review. J Hand Ther. 2026, 39:524-34. 10.1016/j.jht.2025.09.012
2. Valdes K, Naughton N, Algar L: Conservative treatment of mallet finger: a systematic review . J Hand Ther. 2015, 28:237-45; quiz 246. 10.1016/j.jht.2015.03.001
3. Schwartz DA, Schofield KA: Utilization of 3D printed orthoses for musculoskeletal conditions of the upper extremity: a systematic review. J Hand Ther. 2023, 31:166-78. 10.1016/j.jht.2021.10.005
4. Peng C, Huang RW, Chen SH, Hsu CC, Lin CH, Lin YT, Lee CH: Comparative outcomes between surgical treatment and orthosis splint for mallet finger: a systematic review and meta-analysis. J Plast Surg Hand Surg. 2023, 57:54-63. 10.1080/2000656X.2022.2164291
5. Witherow EJ, Peiris CL: Custom-made finger orthoses have fewer skin complications than prefabricated finger orthoses in the management of mallet injury: a systematic review and meta-analysis. Arch Phys Med

Rehabil. 2015, 96:1913-23.e1. 10.1016/j.apmr.2015.04.026
6. Grabau JD, Hoopes HT, Ho C: Upper extremity splint application. J Pediatr Soc North Am. 2025, 12:100239. 10.1016/j.jposna.2025.100239
7. Zolfagharian A, Gregory TM, Bodaghi M, Gharaie S, Fay P: Patient-specific 3D-printed splint for mallet finger injury. Int J Bioprint. 2020, 6:259. 10.18063/ijb.v6i2.259
8. Hou CC, Yi CC, Wu CW, Tsai SL, Huang DW, Tzeng YS: Customized 3-dimensional-printed finger splints for mallet finger. Ann Plast Surg. 2025, 94:S9-12. 10.1097/SAP.0000000000004190
9. Papavasiliou T, Shah RK, Chatzimichail S, Uppal L, Chan JC: Three-dimensional printed customized adjustable mallet finger splint: a cheap, effective, and comfortable alternative. Plast Reconstr Surg Glob Open. 2021, 9:e3500. 10.1097/GOX.0000000000003500
10. Teng SL, Wong YR, Lim PPH, McGrouther DA: An adjustable and customised finger splint to improve mallet finger treatment compliance and outcomes. Ann 3D Print Med. 2024, 13:100142. 10.1016/j.stlm.2024.100142
11. Oud TA, Lazzari E, Gijsbers HJ, Gobbo M, Nollet F, Brehm MA: Effectiveness of 3D-printed orthoses for traumatic and chronic hand conditions: a scoping review. PLoS One. 2021, 16:e0260271. 10.1371/journal.pone.0260271
12. Sedigh A, Kachooei AR, Vaccaro AR, Rivlin M: Contactless remote 3D splinting during COVID-19: report of two patients. J Hand Surg Asian Pac Vol. 2022, 27:398-402. 10.1142/S2424835522720171
13. Sedigh A, Kachooei AR, Beredjiklian PK, Vaccaro AR, Rivlin M: Safety and efficacy of casting during COVID-19 pandemic: a comparison of the mechanical properties of polymers used for 3D printing to conventional materials used for the generation of orthopaedic orthoses. Arch Bone Jt Surg. 2020, 8:281-5.
14. Van Nest DS, Ilyas AM, Rivlin M: Telemedicine evaluation and techniques in hand surgery . J Hand Surg Glob Online. 2020, 2:240-5. 10.1016/j.jhsg.2020.05.006
15. Graham J, Wang M, Frizzell K, Watkins C, Beredjiklian P, Rivlin M: Conventional vs 3-dimensional printed cast wear comfort. Hand (N Y). 2020, 15:388-92. 10.1177/1558944718795291
16. Lebowitz CM, Vosbikian MM, Seigerman DA, et al.: Orthosis material properties: a mechanical testing evaluation of fiberglass, plaster, and three-dimensional printed splints. Plast Reconstr Surg. 2023, 151:179e-81e.
17. Gruber P, Hoppe V, Grochowska E, Paleczny J, Junka A, Smolina I, Kurzynowski T: Material extrusion-based additive manufacturing of poly(lactic acid) antibacterial filaments-a case study of antimicrobial properties. Polymers (Basel). 2021, 13:4337. 10.3390/polym13244337
18. Dadashi A, Azadi M: Multi-objective numerical optimization of 3D-printed polylactic acid bio-metamaterial based on topology, filling pattern, and infill density via fatigue lifetime and mass. PLoS One. 2023, 18:e0291021. 10.1371/journal.pone.0291021
19. Maas SA, Ellis BJ, Ateshian GA, Weiss JA: FEBio: finite elements for biomechanics. J Biomech Eng. 2012, 134:011005. 10.1115/1.4005694
20. Murai S, Tanaka T, Aoki M: Combinatorial roles of extrinsic and intrinsic muscles in extension strength of the distal interphalangeal joint. J Orthop Res. 2012, 30:893-6. 10.1002/jor.22021
21. Dey A, Yodo N: A systematic survey of FDM process parameter optimization and their influence on part characteristics. J Manuf Mater Process. 2019, 3:64. 10.3390/jmmp3030064
22. Peng A, Xiao X, Yue R: Process parameter optimization for fused deposition modeling using response surface methodology combined with fuzzy inference system. Int J Adv Manuf Technol. 2014, 73:87-100. 10.1007/s00170-014-5796-5
23. Torres J, Cotelo J, Karl J, Gordon AP: Mechanical property optimization of FDM PLA in shear with multiple objectives. JOM. 2015, 67:1183-93. 10.1007/s11837-015-1367-y
24. Kim N, Bhalerao I, Han D, Yang C, Lee H: Improving surface roughness of additively manufactured parts using a photopolymerization model and multi-objective particle swarm optimization. Appl Sci. 2019, 9:151. 10.3390/app9010151